CrossMark

Microstructure characterization, stress–strain behavior, superelasticity and shape memory effect of Cu–Al–Mn–Cr shape memory alloys

Shuiyuan Yang[1],*, Fan Zhang[1], Jialin Wu[1], Jinbin Zhang[1], Cuiping Wang[1], and Xingjun Liu[1]

[1] *Fujian Key Laboratory of Materials Genome, College of Materials, Xiamen University, Xiamen 361005, People's Republic of China*

ABSTRACT

In this study, the Cr was added into Cu–Al–Mn alloys for replacing Cu and Mn, and the microstructure, martensitic transformation, stress–strain behavior, superelasticity and shape memory effect of quaternary Cu–Al–Mn–Cr shape memory alloys were investigated. All the studied alloys exhibit a mixed microstructure consisted of dominant $L2_1$ parent, small amounts of A2(Cr) and $2H(\gamma_1')$ martensite, as well as a reversible martensitic transformation. Although the alloys are main $L2_1$ parent before deformation, partial stress-induced $2H(\gamma_1')$ martensite can be stabilized and retained after unloading. Therefore, the same alloy under a certain deformation temperature not only exhibits superelasticity property during deformation, but also the deformed alloy also shows shape memory effect when heated. The results further show that Cu–12.8Al–7.5Mn–2.5Cr alloy has a good superelasticity strain of 2.9% as well as a shape memory effect of 1.5%. Cu–12.7Al–6.9Mn–1.8Cr alloy possesses much the best superelasticity strain close to 5.0% under a pre-deformation of 10% and a shape memory effect of 2.0%. The best shape memory effect up to 2.5% with 10% of pre-deformation and a superelasticity strain of 2.8% are obtained in Cu–12.5Al–5.8Mn–4.1Cr alloy.

Introduction

Shape memory alloys (SMAs) represent a class of advanced smart materials which have several significantly applications in industry and medical fields, such as pipe coupling, actuator and thrombus filter. They have two unique functional properties of shape memory effect (SME) and superelasticity (SE), which both owe to the reversible thermoelastic martensitic transformation [1, 2]. As researched in the early literatures, several types of SMAs have been developed for practical applications, such as NiTi, Cu–Zn–Al, Cu–Al–Ni, Cu–Al–Mn, Fe–Mn–Si [3–9]. Among developed SMAs, NiTi-based alloys are the most commercially important temperature-controlled SMAs due to their excellent SME and SE properties, as well as much better cold workability than that of Cu–Al-based SMAs [1].

Address correspondence to E-mail: yangshuiyuan@xmu.edu.cn

Springer

The Cu–Al-based SMAs have aroused a number of researchers' attentions for their easier fabrication and lower manufacturing cost than those of NiTi-based alloys. The binary Cu–Al-based SMAs undergo an ordered transformation of A2 → B2 → L2$_1$ during cooling [10–12]. With that, a reversible thermoelastic martensitic transformation occurs, and different structural martensite produces, α_1', γ_1' and β_1' depending on the alloy compositions [12, 13]. For those developed Cu–Al-based ternary SMAs, they usually possess a highly ordered L2$_1$ structure and thus exhibit poor cold workability for production and further processing. Additionally, poor thermal stability due to the precipitation of a large amounts of γ_1(Cu$_9$Al$_4$) and α(Cu) phases during aging or thermal cycling is another obstacle for their developments [1, 14–16]. As mentioned in the literatures, the Cu–Al alloys could get an excellent plasticity and large SE strain by alloying Mn, because that Mn addition can decrease the order degree of parent from L2$_1$ structure to A2 structure and widen the composition region of β phase to lower Al concentration [12, 17–19]. Additionally, several investigations on the microstructure and characteristics of ternary Cu–Al–Mn SMAs have been reported so far. Their results show that the grain size has important influences on the SE and SME properties [20–22], as well as the damping capabilities in Cu–Al–Mn SMAs [23]. When the Cu–Al–Mn SMAs have a large relative grain size, they will exhibit a good SE strain. However, the critical stress for stress-inducing martensitic transformation and the fatigue strength of Cu–Al–Mn SMAs are very low, which limit their further practical applications [24, 25]. These problems can be improved by the grain refinement and aging [21, 22, 25]. Alloying is also an effective method to further reinforce the functional properties of Cu–Al–Mn SMAs [19, 21, 26, 27].

For the conventional temperature-controlled SMAs, the occurrence of SME and SE depends on the relationship between the martensitic transformation temperature and deformation temperature [28–34]. The martensite stabilization may be another method to increase the start temperature of reverse martensitic transformation (A_s), except changing alloy compositions. The martensite stabilization is an effect that the A_s temperature of the deformed alloy during heating remarkably raises compared with that without deformation. Picornell et al. reported a mechanical stabilization of stress-induced martensite in Cu–Al–Ni single crystal with large increase in martensitic transformation temperature (about 140 °C). And although the alloy is parent structure before deformation, a permanent residual strain is retained after unloading [35]. Similar phenomena have been also reported in NiTi SMAs [36–38]. In our previous investigation, a new type of Cu–Al–Mn–Fe SMAs is found, having the same "the stabilized stress-induced martensite" phenomenon, in which the A_s temperature raises more than 150 °C [39]. Almost all 2H(γ_1') martensite stress-induced from L2$_1$ parent during deformation could be retained after unloading due to the combined resistances of Fe-rich precipitates and dislocations. Subsequently, large residual strain could completely recover during heating, showing an excellent SME. These findings open a possible avenue to obtain copper-based SMAs having SE and SME characteristics simultaneously, under the same composition and deformation temperature through applying stress.

In Cu–Al–Mn–Fe system [39], it is found that the Fe addition resulting in bcc phase separation of Cu-rich and Fe-rich phases is a necessary condition to stabilize stress-induced 2H(γ_1') martensite. The existence of fine Fe-rich precipitates can hinder the movement of habit plane during reverse transformation. Therefore, we think that the stabilization of stress-induced martensite may also take place in other Cu–Al–Mn-based systems that exist bcc phase separation. Up to now, although Cr-doped Cu–Al–Mn SMAs have been investigated, their works focus on those alloys that a large amounts of Mn replaced Al (Mn: 10–13%, Al: 14–16%, at.% [12]) and have a lower-ordered A2 parent [10, 12, 17]. In this study, higher Al and lower Mn contents were chosen referring to Cu–Al–Mn–Fe alloys in our previous report [39]. In Cu–Cr binary, a metastable liquid two-phase separation exists, and pure Cr is bcc (A2) structure [40]. From Al–Cr and Mn–Cr binary systems, it is found that the bcc A2(Cr) phase has large composition range with Al and Mn elements [41, 42]. So it is estimated that liquid two-phase separation of Cu-rich and Cr-rich phases and the stabilization of stress-induced martensite may also occur in Cu–Al–Mn–Cr system, just like those in the Cu–Al–Mn–Fe system. Therefore, the present study is to investigate the microstructure, martensitic transformation, stress–strain behaviors, SE and SME properties of quaternary Cu–Al–Mn–Cr alloys.
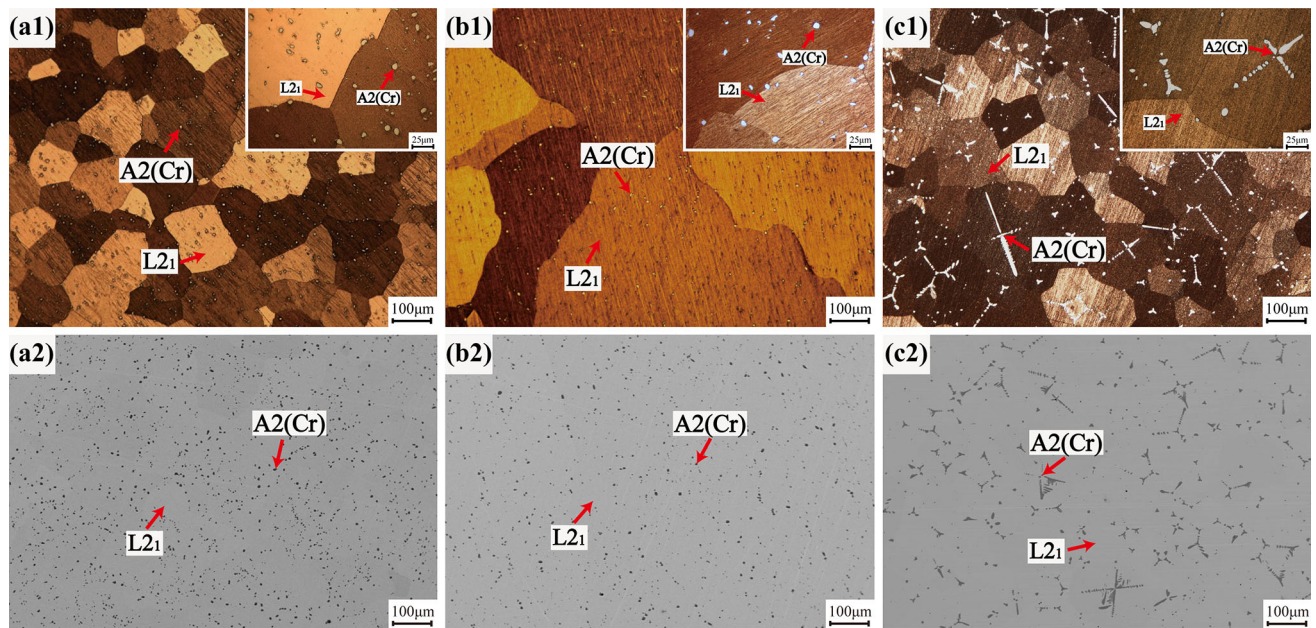
Figure 1 Optical micrographs and the corresponding BSE images of **a1**, **a2** Cu–12.8Al–2.5Cr–7.5Mn alloy, **b1**, **b2** Cu–12.7Al–1.8Cr–6.9Mn alloy and **c1**, **c2** Cu–12.5Al–4.1Cr–5.8Mn alloy.

Experimental

Materials preparation

Three samples with the chemical compositions of Cu–12.8Al–7.5Mn–2.5Cr, Cu–12.7Al–6.9Mn–1.8Cr and Cu–12.5Al–5.8Mn–4.1Cr (wt%) alloys were prepared. Pure raw materials were provided by General Research Institute for Nonferrous Metals. The purities of Cu, Al, Mn and Cr are 99.95, 99.99, 99.7 and 99.98%, respectively. Firstly, the raw materials were cut and ultrasonic cleared with acetone, in which Mn previously needed acid pickling. Then, about 30 g raw materials was put into a water-cooled copper crucible and re-melted using a non-consumable tungsten electrode with a current range about 250–400 A. During melting process, each button was turned over and re-melted for five times in a high-purity argon atmosphere in order to make sure the uniformity of samples. Each sample was cut into small bulks. These small bulks were sealed into vacuum quartz ampoules. In this study, in order to make the studied alloys be solution-treated in the parent region, the temperature and time of heat treatment were chosen to be 900 °C and 24 h referring to the investigations of Cu–Al–Mn by Kaimuna [17] and Cu–Al–Fe–Mn alloys by our group [39]. Then, the heat-treated vacuum quartz ampoules were quickly quenched into ice water.

Materials characterization

The chemical compositions were determined by electron probe microanalysis (EPMA) (JEOL, JXA–8100). The microstructure was observed by optical microscopy (OM), back-scattered electron (BSE). Samples for microscopic observation were mechanically polished and chemically etched (10 g $FeCl_3$ + 25 ml HCl + 100 ml H_2O). The crystal structure was identified by PANalytical X'pert PRO X-ray diffractometer with Cu Kα radiation. The X-ray diffraction patterns were analyzed using Jade 6.0 software and the previously reported references. The martensitic transformation temperatures were determined by differential scanning calorimetry (DSC) at a heating and cooling rate of 10 °C min^{-1}. The scanning rate of the DSC tests is 30 pts/K.

The stress–strain behaviors and shape recovery properties were performed by compressive tests. The cylindrical specimens of 3 mm diameter and 5 mm height were cut from the quenched bulks. Five samples were prepared, and then, each sample was deformed to different pre-deformation from 7 to 11% at room temperature, respectively. The SE properties

Table 1 Chemical compositions of L2₁ parent and A2(Cr) phase in Cu–Al–Mn–Cr alloys

Alloys	L2$_1$ (wt%)				A2(Cr) (wt%)			
	Cu	Al	Cr	Mn	Cu	Al	Cr	Mn
Cu–12.8Al–7.5Mn–2.5Cr	79.26	13.06	0.61	7.06	3.17	5.58	83.31	7.94
Cu–12.7Al–6.9Mn–1.8Cr	79.67	12.93	0.78	6.62	3.03	4.62	84.61	7.74
Cu–12.5Al–5.8Mn–4.1Cr	80.79	12.69	0.46	6.06	2.17	4.31	89.04	4.48

were confirmed and calculated directly by stress–strain curves as adopted in [24]. For those samples having the residual strain after unloading, their SMEs were measured by thermal mechanical analysis (TMA) under an argon atmosphere at a heating and cooling rate of 10 °C min^{-1}. In Cu–Al binary system,

the eutectoid reaction leading to the precipitation of γ_1(Cu$_9$Al$_4$) phase occurs about 567 °C [41]. Therefore, in order to investigate the stability of martensitic transformation, the temperature range of TMA tests was from room temperature to 600 °C. Then, the microstructural evolution after TMA tests was investigated. The height of the sample was measured before loading (h_0), after unloading (h_1) and after recovery (h_2). The SMEs (ε_{SME}) and recovery rates after heating were calculated as $\varepsilon_{SME} = (h_2 - h_1)/h_0 \times 100\%$ and rate $= (h_2 - h_1)/(h_0 - h_1) \times 100\%$, respectively [12, 13, 16].
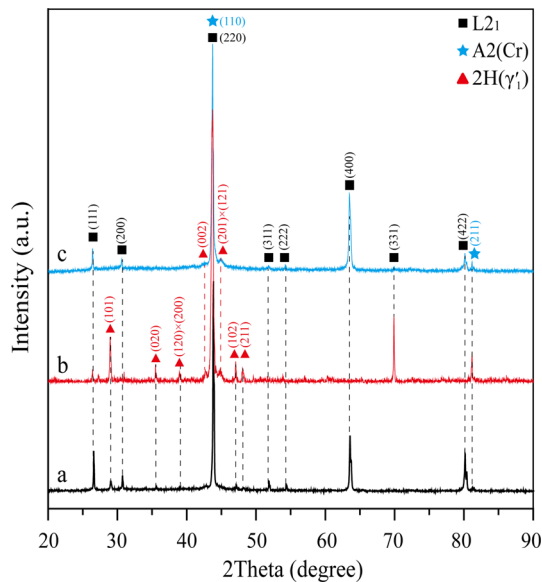

Figure 2 X-ray diffraction patterns of *a* Cu–12.8Al–2.5Cr–7.5Mn alloy, *b* Cu–12.7A–1.8Cr–6.9Mn alloy and *c* Cu–12.5Al–4.1Cr–5.8Mn alloy.

Results and discussion

Microstructure characteristics

Figure 1 shows the optical micrographs and the corresponding BSE images of the studied alloys. It can be seen that three alloys consist of the parent and some small amounts of precipitates. Both in Cu–12.8Al–7.5Mn–2.5Cr and Cu–12.7Al–6.9Mn–1.8Cr alloys, the precipitates dispersively distribute within the parent. When increasing the Cr content, the amounts of precipitates clearly increase, and they converge progressively to a cross-shape in Cu–12.5Al–5.8Mn–4.1Cr alloy. These results are
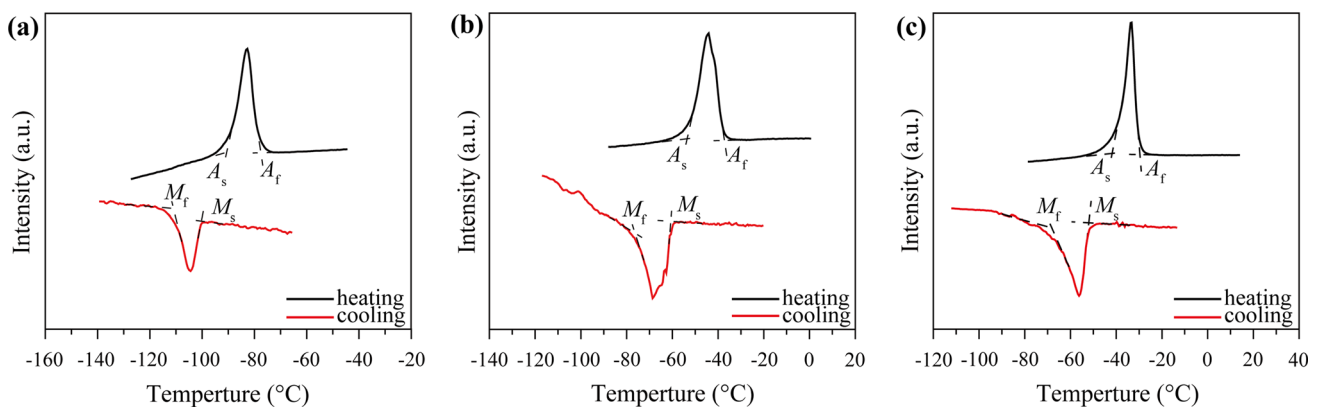

Figure 3 DSC curves of **a** Cu–12.8Al–2.5Cr–7.5Mn alloy, **b** Cu–12.7Al–1.8Cr–6.9Mn alloy and **c** Cu–12.5Al–4.1Cr–5.8Mn alloy.

Table 2 Martensitic transformation temperatures (°C) of Cu–Al–Mn–Cr alloys. M_s and M_f are the start and finish temperatures of forward martensitic transformation; A_s and A_f are the start and finish temperatures of reverse martensitic transformation

Alloys	M_s	M_f	A_s	A_f	Hysteresis
Cu–12.8Al–7.5Mn–2.5Cr	−100.2	−111	−90.6	−77.5	22.7
Cu–12.7Al–6.9Mn–1.8Cr	−60.7	−76.3	−53.3	−37.3	23.4
Cu–12.5Al–5.8Mn–4.1Cr	−51.9	−68.2	−41.8	−29.7	22.2
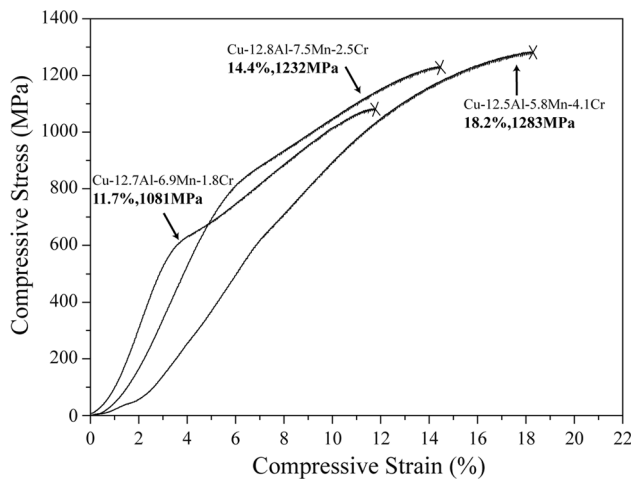
Figure 4 Compressive fracture stress–strain curves of Cu–Al–Mn–Cr alloys.

obviously observed in the corresponding BSE images in Fig. 1a2–c2. The chemical compositions of each phase in the studied alloys were determined by EPMA measurements and are shown in Table 1. Figure 2 shows the XRD patterns of the studied Cu–Al–Mn–Cr alloys. Three crystal structures are identified. The parent has a L2$_1$ structure, and A2(Cr) precipitate is also confirmed. Additionally, the diffraction peaks of 2H(γ_1') martensite are observed. From our previous investigation [39], it is found that the 2H(γ_1') martensite formed due to direct quenching process is very fine in Cu–Al–Mn–Fe alloys. Similarly in this study, the 2H(γ_1') martensite cannot be observed in their optical micrographs in Fig. 1. These results are agreed with those reports in Cu–Al–Mn–Fe alloys [39]. According to phase equilibria of Cr–Cu/Al/Mn binary systems [40–42], the metastable liquid phase two-phase (the Cu-rich and Cr-rich phases) separation occurs. When the Cu–Al–Mn–Cr alloys cool from the liquid, the Cu-rich phase transforms to L2$_1$ parent via the ordered transformations of A2 → B2 → L2$_1$ [10, 12], and the A2 (Cr-rich) forms from the rich-Cr liquid [40]. These results are consistent with what we expected.

Martensite transformation temperature

Figure 3 shows the DSC curves of the studied three alloys with a heating and cooling rate of 10 °C min^{-1}. The reversible martensitic transformation peaks are clearly observed. As shown in Table 2, the start (M_s) and finish (M_f) temperatures of forward martensitic transformation are −100.2 and −111.0 °C for Cu–12.8Al–7.5Mn–2.5Cr alloy, −60.7 and −76.3 °C for Cu–12.7Al–6.9Mn–1.8Cr alloy, −51.9 and −68.2 °C for Cu–12.5Al–5.8Mn–4.1Cr alloy, respectively. The start (A_s) and finish (A_f) temperatures of reverse martensitic transformation are −90.6 and −77.5 °C for Cu–12.8Al–7.5Mn–2.5Cr alloy, −53.3 and −37.3 °C for Cu–12.7A–6.9Mn–1.8Cr alloy, −41.8 and −29.7 °C for Cu–12.5Al–5.8Mn–4.1Cr alloy, respectively. The transformation thermal hysteresis is calculated using the formula: A_f–M_s. As we known, the reversible martensitic transformation temperatures of Cu–Al–Mn SMAs sharply decrease with the increases both in the Mn and Al contents [21, 26, 27]. The Cr addition in Cu–Al–Mn alloys also decreases the transformation temperatures with a lower rate than the effects of Mn or Al contents [26]. In the present study, according to the compositions of L2$_1$ parent in Table 1, the same results as the previous reports that the martensitic transformation temperatures gradually increase with the decrease in Mn and Al contents are present.

Compression test

Figure 4 shows the compressive fracture stress–strain curves of Cu–Al–Mn–Cr alloys. The symbol (×) represents the fracture point. The compressive fracture stress and strain were measured to be 14.4% and 1232 MPa for Cu–12.8Al–7.5Mn–2.5Cr alloy, 11.7% and 1081 MPa for Cu–12.7Al–6.9Mn–1.8Cr alloy, 18.2% and 1283 MPa for Cu–12.5Al–4.1Cr–5.8Mn alloy, respectively. Cu–12.7Al–6.9Mn–1.8Cr alloy has a relatively lower fracture plasticity than other two alloys due to a larger grain size (Fig. 1). With

increasing the amounts of A2(Cr) precipitate for Cu–12.5Al–5.8Mn–4.1Cr alloy, the plasticity also increases accordingly.

Superelasticity and shape memory effect

In order to investigate the SE and SME properties in Cu–Al–Mn–Cr alloys. Each alloy was compressed to different pre-strains (ε_{pre}) from 7 to 11% and unloading. Figure 5 shows the compressive stress–strain curves of the studied alloys. The SE strain (ε_{SE}) is directly measured from the stress–strain curves. The deformed samples were heated to 600 °C for 5 min with a heating and cooling rate of 10 °C min^{-1} using TMA tests. Then, the SME strain (ε_{SME}) was obtained through measuring the height changes of the samples (See the Experimental procedure). All the residual strain (ε_r) after unloading, ε_{SE} and ε_{SME} are summarized and their relationships with the total ε_{pre} are shown in Fig. 6.

From Fig. 5, the SE properties are observed for all the studied alloys. In Cu–12.8Al–7.5Mn–2.5Cr alloy,

the residual strain almost linearly increases with the increase in the pre-strain, but the SE strain decreases from 2.9 to 2.1%. Similar stress–strain behaviors exist in Cu–12.5Al–5.8Mn–4.1Cr alloy. According to the increase in the pre-strain from 7 to 11%, the residual strain increases from 1.0 to 5.0%, but the SE strain decreases from 2.8 to 2.1%. There are some differences on the stress–strain behaviors of Cu–12.7Al–6.9Mn–1.8Cr alloy in Fig. 5b, showing much more excellent SE properties. When the pre-strain is ≤10%, the SE strain gradually increases to a maximum value of about 5.0%, while the residual strain is ≤0.9%. When increasing the pre-strain to 11%, the SE strain suddenly reduces to 2.6%, whereas the residual strain rises to 3.9%.

It is interesting when the deformed samples after unloading are heated, the residual strain can recover, namely SME. The SMEs gradually increase from 0.7 to 1.5% according to the increase in the pre-strain from 7 to 11% for Cu–12.8Al–7.5Mn–2.5Cr alloy. Cu–12.5Al–5.8Mn–4.1Cr alloy shows much better SMEs,
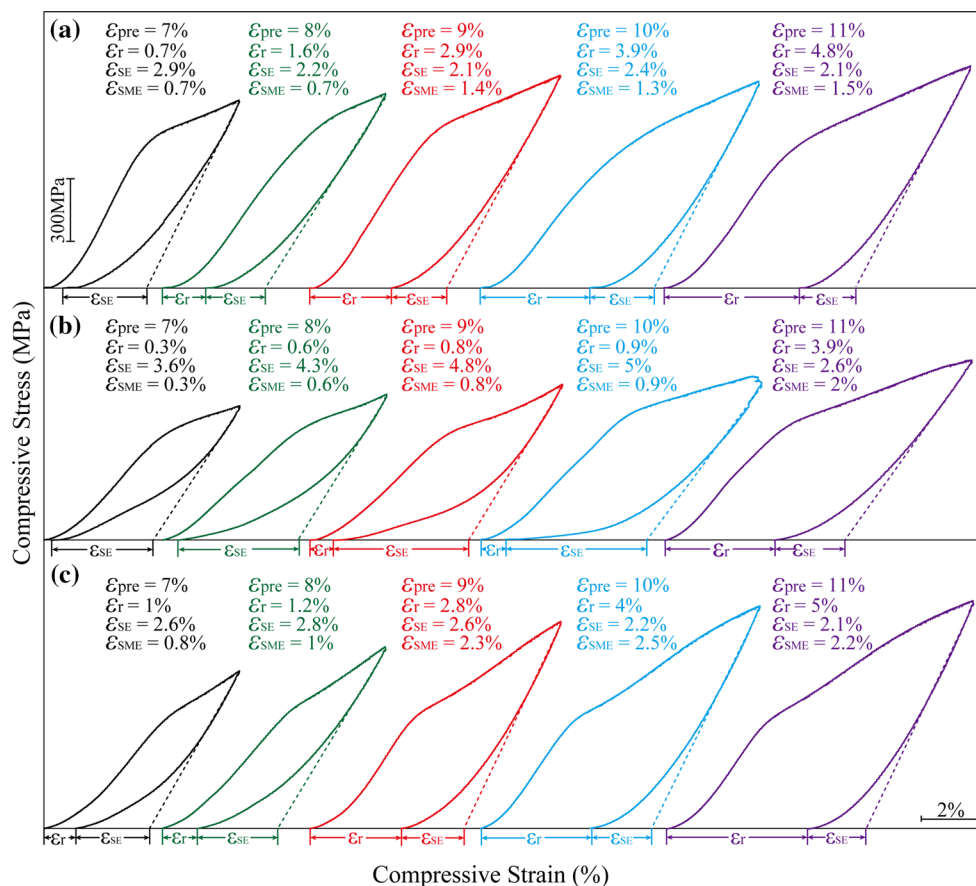
Figure 5 Compressive stress–strain curves of **a** Cu–12.8Al–7.5Mn–2.5Cr alloy, **b** Cu–12.7Al–6.9Mn–1.8Cr alloy and **c** Cu–12.5Al–5.8Mn–4.1Cr alloy.
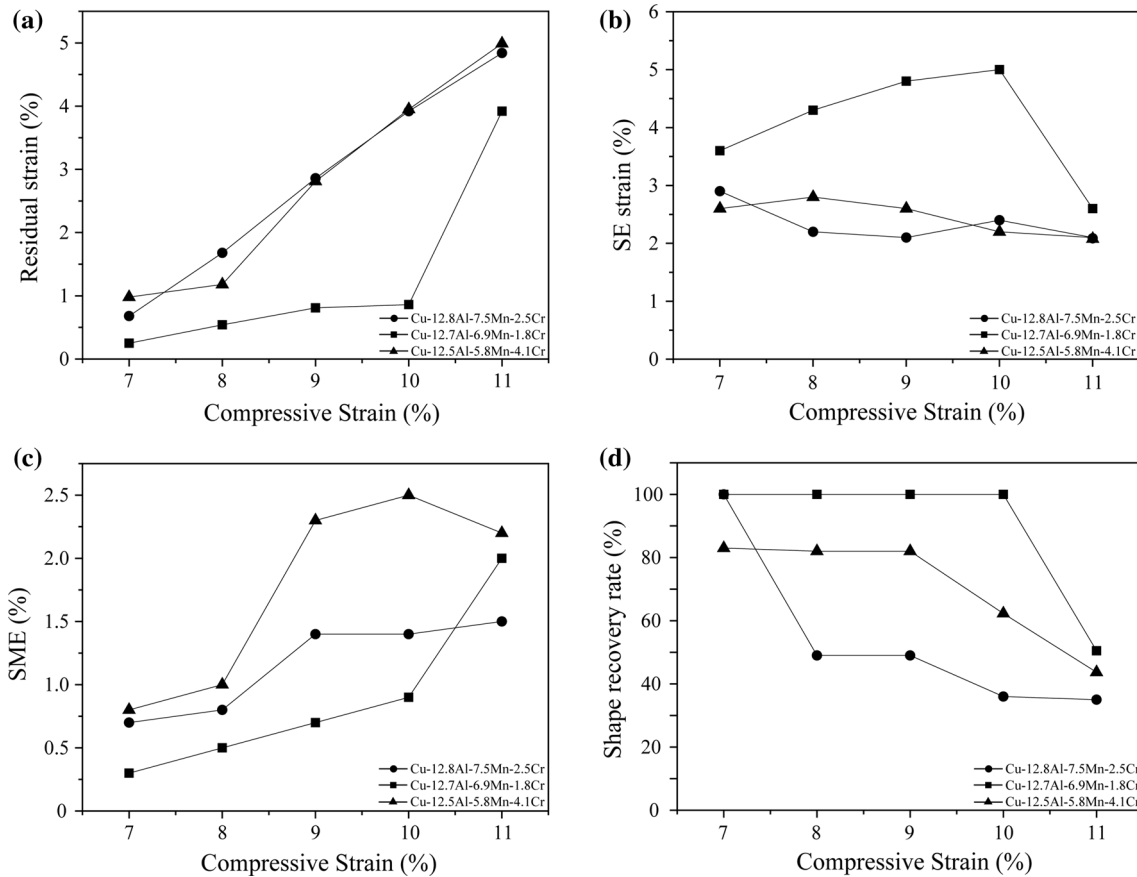
Figure 6 a Residual strain, **b** SE strain, **c** SME, **d** shape recovery rate of Cu–Al–Mn–Cr alloys as a function of the pre-strain.
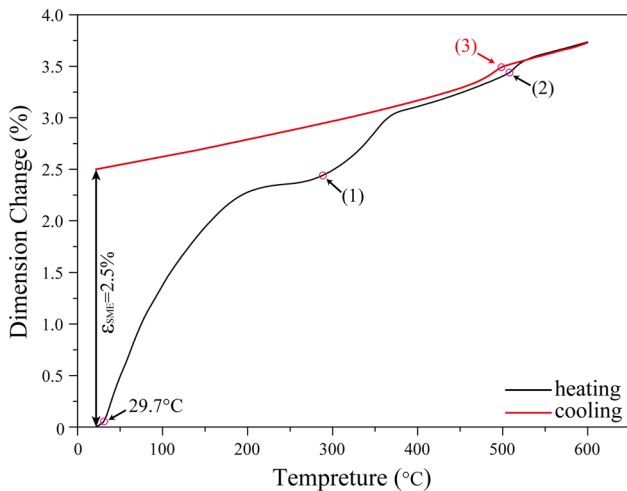

Figure 7 TMA curve of Cu–12.5Al–4.1Cr–5.8Mn alloy with a heating and cooling rate of 10 °C min⁻¹, in which the alloy is deformed to a pre-strain strain of 10% and unloading.

in which the largest SME is about 2.5% under a pre-strain of 10%. Small SME of 0.9% is obtained even the pre-strain is up to 10% for Cu–12.7Al–6.9Mn–1.8Cr

alloy. However, this alloy possesses a large SME of about 2.0% when the pre-strain increases to 11%. The shape recovery rate of Cu–12.8Al–7.5Mn–2.5Cr alloy due to SME property during heating clearly decreases. The recovery rate of Cu–12.7Al–6.9Mn–1.8Cr alloy is almost 100% when the pre-strain is ≤10%, but decreases to 51% when the deformation further increases to 11%. The shape recovery rate of Cu–12.5Al–5.8Mn–4.1Cr alloy is between the above two alloys. When the pre-strain is ≤9%, the recovery rate is about 80% and gradually decreases to 44% with the increase in the deformation. From the results in Figs. 5 and 6, it is found that the stress–strain and shape recovery properties of the present Cu–Al–Mn–Cr alloys are similar to those of the reported Cu–Al–Mn–Fe alloys [39]. Although the Cu–Al–Mn–Cr alloys are dominant L2₁ parent before deformation, the same alloy under a certain deformation temperature not only exhibits superelasticity property during deformation, but also the deformed alloy also shows shape memory effect when heated.

🖄 Springer
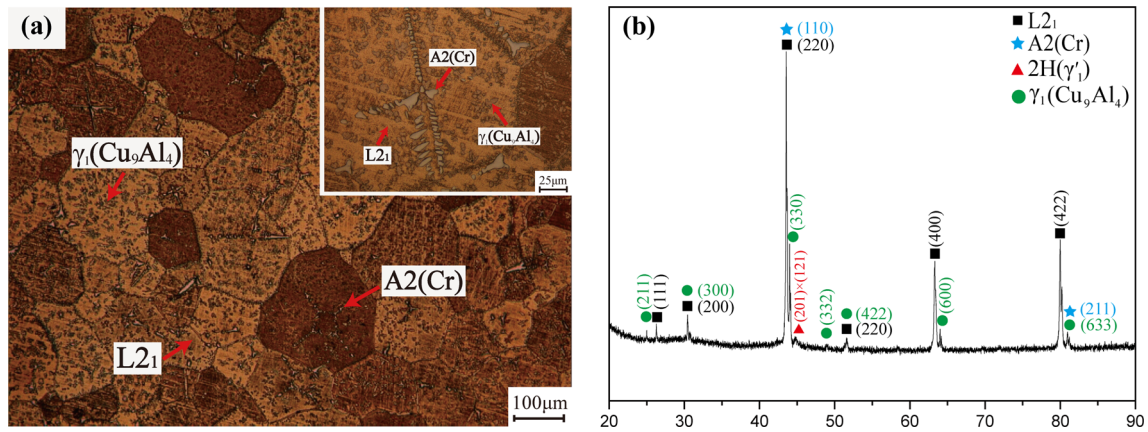
Figure 8 Optical micrograph **a** and X-ray diffraction pattern **b** of Cu–12.5Al–5.8Mn–4.1Cr alloy annealed at 500 °C for 3 h and air cooling to room temperature.
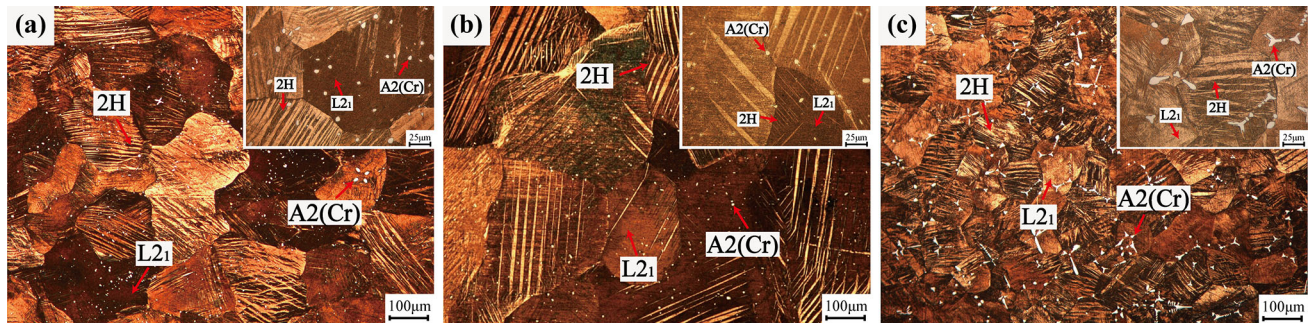
Figure 9 Microstructures of **a** Cu–12.8Al–2.5Cr–7.5Mn alloy, **b** Cu–12.7Al–1.8Cr–6.9Mn alloy and **c** Cu–12.5Al–4.1Cr–5.8Mn alloy, in which three alloys are compressed to a pre-strain of 10% and unloading.

Thermal mechanical analysis

Figure 7 shows the shape recovery curve of the Cu–12.5Al–5.8Mn–4.1Cr alloy deformed to 10% and after unloading measured by TMA test. The start temperature for shape recovery due to reverse martensitic transformation is about 29.7 °C. Here, a remarkable martensite stabilization is observed, in which the shift of start temperature of reverse martensitic transformation (A_s) is about 71.5 °C. Additional three transformation peaks shown by the arrows in Fig. 7 are observed. In order to investigate these transformations, Cu–12.5Al–5.8Mn–4.1Cr alloy was aging at 500 °C for 3 h and air cooling to room temperature. Then, the microstructural evolution was observed, and the results are given in Fig. 8. We find that three transformation peaks may be related to the precipitation and dissolution of $\gamma_1(Cu_9Al_4)$ phase. From Fig. 8a, it is seen that some precipitates

appear along the grain boundaries or within the grain, except the parent and A2(Cr) phase. Its chemical composition is $Cu_{66.38}Al_{30.06}Mn_{2.85}Cr_{0.71}$ (at%), which accords to that of the compound γ_1-(Cu_9Al_4) phase in Cu–Al-based SMAs [13, 16]. The diffraction peaks of $\gamma_1(Cu_9Al_4)$ phase are also identified in Fig. 8b. Combined with the results in Fig. 7, the deformation process may lead that this precipitation is more likely to happen at lower temperature (below 500 °C), as shown by the arrow (1). Subsequently, this alloy annealed from 500 °C was further heat-treated at 750 °C for 3 h and followed by ice-water quenching. The compound $\gamma_1(Cu_9Al_4)$ dissolves back to L2$_1$ parent, and the corresponding microstructure is the same as that in Fig. 1c1. This dissolution process of $\gamma_1(Cu_9Al_4)$ phase is indicated by the peak (2) during heating. The precipitation of $\gamma_1(Cu_9Al_4)$ phase during cooling with a slow rate may occur as shown by the peak (3).

Stabilization of stress-induced martensite

In order to uncover the SME behaviors of the present Cu–Al–Mn–Cr alloys, three alloys were deformed to a pre-strain of 10% and unloading. The microstructures of the deformed alloys as shown in Fig. 9 clearly differ from those before deformation (Fig. 1). A martensite feature is observed after deformation and unloading in Fig. 9, whereas is main $L2_1$ parent before deformation in Fig. 1. The results imply that the stabilization of stress-induced martensite happens in Cu–Al–Mn–Cr alloys during deformation and unloading. The corresponding X-ray diffraction pattern of the deformed alloys is provided in Fig. 10, in which the intensities of the diffraction peaks of $2H(\gamma_1')$ martensite clearly reinforce. The occurrence of stabilization of stress-induced martensite results from the precipitates and the dislocation induced by compression deformation restrain the movement of the habit plane [39]. Thus, the reverse martensitic transformation does not take place during unloading, whereas it occurs when the deformed alloys are heated. Although the "stabilized stress-induced martensite" phenomenon is consistent with those findings in reported Cu–Al–Mn–Fe alloys [39], the SE or SME strains of Cu–Al–Mn–Cr alloys are clearly
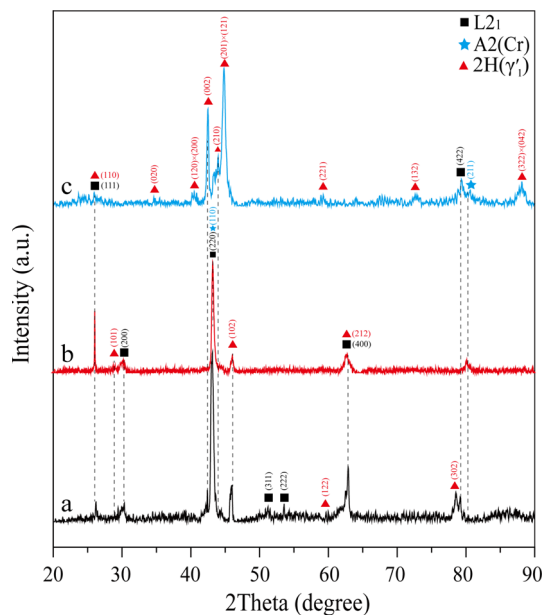
Figure 10 X-ray diffraction patterns of *a* Cu–12.8Al–2.5Cr–7.5Mn alloy, *b* Cu–12.7Al–1.8Cr–6.9Mn alloy, *c* Cu–12.5Al–4.1Cr–5.8Mn alloy, in which three alloys are compressed to a pre-strain of 10% and unloading.

smaller compared with the Cu–Al–Mn–Fe alloys. This is closely relative to the grain size of $L2_1$ parent [22, 39]. For Cu–Al–Mn–Fe alloys [39], it is found when the alloys exhibit excellent SE and SME properties, they usually have a very large grain size. Therefore, it is suggested if we want to obtain more excellent SE or SME properties induced by the stabilization of stress-induced martensite, the preparation of single crystal or large grain structure may be an effective method, such as a cyclic heat treatment in Cu–Al–Mn ternary alloys [43].

From Figs. 1 and 9, it can be seen that the grain size of $L2_1$ parent gradually decreases with the increases in the Cr addition and the A2(Cr) phase amounts. The best SE characteristic is obtained in Cu–12.7Al–6.9Mn–1.8Cr alloy with the largest grain size of parent. Meanwhile, almost 100% shape recovery rate is obtained with the pre-strain ≤10%. In Figs. 9 and 10, under the same pre-strain of 10%, less amounts of 2H martensite are induced and stabilized in Cu–12.7Al–6.9Mn–1.8Cr alloy. Only when the deformation increases to 11%, more obvious stabilization of stress-induced martensite occurs along. At this time, the SME clearly increases, but recovery rate drastically reduces due to the plastic deformation. For Cu–12.8Al–7.5Mn–2.5Cr and Cu–12.5Al–5.8Mn–4.1Cr alloys, with the increase in the pre-strain, the SE strain gradually decreases, whereas the SME increases with a decreasing shape recovery rate due to the plastic deformation. However, it is found that the SME properties are much better in Cu–12.5Al–5.8Mn–4.1Cr alloy than those of Cu–12.8Al–7.5Mn–2.5Cr alloy. The reason may be related to the reversible martensitic transformation temperatures of the alloys. When the transformation temperature is lower, the needed stress to stabilize the stress-induced martensite is much higher. It will produce more plastic deformation, resulting in a decrease in SMEs of the alloys.

Conclusions

In this study, the microstructure, martensitic transformation, stress–strain behaviors, SE and SME properties of Cu–12.8Al–7.5Mn–2.5Cr, Cu–12.7Al–6.9Mn–1.8Cr and Cu–12.5Al–5.8Mn–4.1Cr SMAs were investigated. The obtained results lead to the following conclusions:

(1) Three alloys have a complex microstructure consisted of dominant $L2_1$ parent, small amounts A2(Cr) and $2H(\gamma_1')$ martensite. With the increase in the Cr content, the amounts of A2(Cr) phase increase accordingly, and the grain size of $L2_1$ parent decreases. The reversible martensitic transformation temperatures gradually increase with the decreases in Al and Mn concentrations.

(2) Three alloys exhibit different SE properties. With the increase in the deformation, the SE strain gradually decreases from about 2.9 to 2.1%. Cu–12.7Al–6.9Mn–1.8Cr alloy exhibits much better SE properties due to a larger grain size of $L2_1$ parent. The SE strain increases to a largest value of about 5% with a pre-strain of 10%. Further increasing the deformation to 11%, the SE strain decreases due to the plastic deformation.

3) Although three alloys are dominant $L2_1$ parent before deformation, the stabilization of stress-induced $2H(\gamma_1')$ martensite happens. When the deformed alloys are heated, the residual strain recovers, showing SME properties. When increasing the pre-strain, the SME gradually increases up to the largest values of 1.5 and 2.5% with the decreasing recovery rate in Cu–12.8Al–7.5Mn–2.5Cr and Cu–12.5Al-5.8Mn–4.1Cr alloys. For Cu–12.7Al–6.9Mn–1.8Cr alloy, almost 100% of recovery rate is obtained when the pre-strain is ≤10%. Further increasing the deformation to 11%, the SME increases to 2% while the recovery rate drastically decreases.

Acknowledgements

References

[1] Otsuka K, Wayman CM (1998) Shape memory materials. Cambridge University Press, Cambridge

[2] Otsuka K, Shimizu K (1986) Pseudoelasticity and shape memory effects in alloys. Int Met Rev 31:93–114

[3] Otsuka K, Ren XB (1999) Recent developments in the research of shape memory alloys. Intermetallics 7:511–528

[4] Otsuka K, Ren X (2005) Physical metallurgy of Ti–Ni-based shape memory alloys. Prog Mater Sci 50:511–678

[5] Bonnot E, Romero R, Morin M et al (2008) In-situ observations of a martensitic transformation in a Cu–Zn–Al single crystal driven by stress or strain. J Mater Sci 43:3832. doi:10.1007/s10853-007-2218-1

[6] Sarı U, Kırındı T (2008) Effects of deformation on microstructure and mechanical properties of a Cu–Al–Ni shape memory alloy. Mater Charact 59:920–929

[7] Araki Y, Endo T, Omori T, Sutou Y In-situ observations of a martensitic transformation in a Cu–Zn–Al single crystal driven by stress or strain at springer link, Koetaka Y, Kainuma R et al (2011) Potential of superelastic Cu–Al–Mn alloy bars for seismic applications. Earthq Eng Struct Dyn 40:107–115

[8] Stanford N, Dunne DP (2007) Martensite/particle interactions and the shape memory effect in an Fe–Mn–Si-based alloy. J Mater Sci 42:4334–4343. doi:10.1007/s10853-006-0686-3

[9] Liu Y, Van Humbeeck J, Stalmans R, Delaey L (1997) Some aspects of the properties of NiTi shape memory alloy. J Alloy Compd 247:115–121

[10] Kainuma R, Satoh N, Liu XJ, Ohnuma I, Ishida K (1998) Phase equilibria and Heusler phase stability in the Cu-rich portion of the Cu–Al–Mn system. J Alloy Compd 266:191–200

[11] Xu HB (2001) Cu-based high-temperature shape-memory alloys and their thermal stability. Mater Sci Forum 394–3:375–382

[12] Kainuma R, Takahashi S, Ishida K (1996) Thermoelastic martensite and shape memory effect in ductile Cu–Al–Mn alloys. MMTA 27:2187

[13] Yang SY, Su Y, Wang CP, Liu XJ (2014) Microstructure and properties of Cu–Al–Fe high-temperature shape memory alloys. Mater Sci Eng B 185:67–73

[14] Matlakhova LA, Pereira EC, Matlakhov AN, Monteiroa SN, Toledo R (2008) Mechanical behavior and fracture characterization of a monocrystalline Cu–Al–Ni subjected to thermal cycling treatments under load. Mater Charact 59:1630–1637

[15] Nakata Y, Tadaki T, Shimizu K (1985) Thermal cycling effects in a Cu–Al–Ni shape memory alloy. J Jpn Inst Met 26:646–652

[16] Wang CP, Su Y, Yang SY, Shi Z, Liu XJ (2014) A new type of Cu–Al–Ta shape memory alloy with high martensitic transformation temperature. Smart Mater Struct 23:025018–1–025018–7

[17] Kainuma R, Takahashi S, Ishida K (1995) Ductility shape memory alloys of the Cu–Al–Mn system. J de Phys IV 5:961–966

[18] Mallik US, Sampath V (2008) Influence of aluminum and manganese concentration on the shape memory characteristics of Cu–Al–Mn shape memory alloys. J Alloy Compd 59:142–147

[19] Mallik US, Sampath V (2008) Effect of alloying on microstructure and shape memory characteristics of Cu–Al–Mn shape memory alloys. Mater Sci Eng A 481–482:680–683

[20] Oliveira JP, Panton B et al (2016) Laser welded superelastic Cu–Al–Mn shape memory alloy wires. Mater Des 90:122–128

[21] Sutou Y, Omori T, Okamoto T, Kainuma R, Ishida K (2001) Effect of grain refinement on the mechanical and shape memory properties of Cu–Al–Mn base alloys. J Phys IV France 11:185–190

[22] Sutou Y, Omori T, Kainuma R, Ishida K (2013) Grain size dependence of pseudoelasticity in polycrystalline Cu–Al–Mn-based shape memory sheets. Acta Mater 61:3842–3850

[23] Oliveira JP, Zeng Z et al (2016) Improvement of damping properties in laser processed superelastic Cu–Al–Mn shape memory alloys. Mater Des 98:280–284

[24] Sutou Y, Koeda N, Omori T, Kainuma R, Ishida K (2009) Effects of aging on stress-induced martensitic transformation in ductile Cu–Al–Mn-based shape memory alloys. Acta Mater 57:5759–5770

[25] Sutou Y, Koeda N, Omori T, Kainuma R, Ishida K (2009) Effects of aging on bainitic and thermally induced martensitic transformation in ductile Cu–Al–Mn-based shape memory alloys. Acta Mater 57:5748–5758

[26] Sutou Y, Kainuma R, Ishida K (1999) Effect of alloying elements on the shape memory properties of ductile Cu–Al–Mn alloys. Mater Sci Eng A 273–275:375–379

[27] Mallik US, Sampath V (2009) Influence of quaternary alloying additions on transformation temperatures and shape memory properties of Cu–Al–Mn shape memory alloy. J Alloy Compd 469:156–163

[28] Ma YQ, Yang SY, Liu Y, Liu XJ (2009) The ductility and shape-memory properties of Ni–Mn–Co–Ga high-temperature shape-memory alloys. Acta Mater 57:3232–3241

[29] Canbay CA, Gudeloglu S, Genc ZK (2015) Investigation of the enthalpy/entropy variation and structure of Cu–Al–Mn–Fe shape memory alloys. Int J Thermophys 36:783–794

[30] Ortin J, Planes A (1988) Thermodynamic analysis of thermal measurements in thermoelastic martensitic transformations. Acta Metall 36:1873–1889

[31] Canbay CA, Aydogdu A (2013) Thermal analysis of Cu–14.82 wt% Al–0.4 wt% Be shape memory alloy. J Therm Anal Calorim 113:731–737

[32] Kainuma R et al (2006) Magnetic-field-induced shape recovery by reverse phase transformation. Nature 439:957–959

[33] Tanaka Y et al (2010) Ferrous polycrystalline shape-memory alloy showing huge superelasticity. Science 327:1488–1490

[34] Otsuka K, Wayman CM, Nakai K, Sakamota H, Shimizu K (1976) Superelasticity effects and stress-induced martensitic transformations in Cu–Al–Ni alloys. Acta Metall 24:207–226

[35] Picornell C, Pons J, Cesari E (2001) Stabilization of martensite by applying compressive stress in Cu–Al–Ni single crystals. Acta Mater 49:4221–4230

[36] Sedmák P, Šittner P, Pilch J, Curfs C (2015) Instability of cyclic superelastic deformation of NiTi investigated by synchrotron X-ray diffraction. Acta Mater 94:257–270

[37] Oliveira JP, Miranda RM, Schell N, Fernandes FMB (2016) High strain and long duration cycling behavior of laser welded NiTi sheets. Int J Fatigue 83:195–200

[38] Oliveira JP, Fernandes FMB, Schell N, Miranda RM (2016) Martensite stabilization during superelastic cycling of laser welded NiTi plates. Mater Lett 171:273–276

[39] Yang SY, Omori T, Wang CP, Liu Y, Makoto N et al (2016) A jumping shape memory alloy under heat. Sci Rep 6:21754

[40] Villars P, Calvert LD (1991) Pearson's handbook of crystallographic data for intermetallic phases, 2nd edn. ASM, Materials Park

[41] Massalski TB (1990) Binary alloy phase diagrams, 2nd edn. ASM International, Metals Park

[42] Lee BJ (1993) A thermodynamic evaluation of the Cr–Mn and Fe–Cr–Mn systems. Metall Trans A 24A:1919–1933

[43] Omori T, Kusama T et al (2013) Abnormal grain growth induced by cyclic heat treatment. Science 341:1500–1502